CANCER
COMMUNICATIONS Open Access

LETTER TO THE EDITOR

Plasma small-extracellular vesicles enriched in miR-122-5p promote disease aggressiveness in pediatric anaplastic large-cell lymphoma

Dear Editor,

Anaplastic lymphoma kinase-positive (ALK$^+$) anaplastic large cell lymphoma (ALCL) is an aggressive peripheral T-cell lymphoma representing 10%-15% of pediatric lymphoid neoplasms. The constitutively activated nucleophosmin-ALK (NPM-ALK) fusion protein is the main driver of ALK$^+$ ALCL oncogenesis [1]. Current clinical protocols can achieve high cure rates, with 75% event-free survival (EFS) at 5 years [2], but the patients' outcome with relapsed/refractory disease still remains poor [3]. Liquid biopsy is widely applied for the prognostic and therapeutic stratification of onco-hematological patients. As a non-invasive procedure, it can be used to identify several biomarkers, such as small extracellular vesicles (S-EVs) [4]. S-EVs are stable carriers of molecules that mediate genetic exchange between distant cells, alter the microenvironment, facilitate cancer cell progression and promote drug resistance [5].

To investigate the role of S-EVs-delivered microRNAs (miRNAs) as disease biomarkers and their function in pediatric ALCL, we identified plasma S-EVs miRNA profile by small RNA-sequencing (sRNA-seq) in a panel of NPM-ALK$^+$ ALCL patients ($n = 20$) and healthy donors (HD) ($n = 5$). All ALCL patients included in the study were NPM-ALK$^+$; henceforth, we will refer to them as "ALCL". The patients' baseline characteristics are shown in Supplementary Table S1. Bioinformatics analysis using the

miR&moRe2 software [6] showed distinct miRNA profiles between ALCL and HD (Figure 1A) with 12 miRNAs significantly enriched in ALCL S-EVs (Supplementary Figure S1A and Supplementary Table S2). For further investigations, we focused on miR-122-5p since it is involved in the dissemination of adult solid tumors [7]. miR-122-5p enrichment in plasma S-EVs of an extended cohort of ALCL ($n = 66$) patients and HD ($n = 19$) was validated (Figure 1B), and the highest levels were detected in patients with disease dissemination (stage III-IV) (Figure 1B). Of note, comparing miR-122-5p levels in ALCL plasma S-EVs with patient-matched tumor biopsies, we found that miR-122-5p was barely detectable in ALCL lymph nodes according to both sRNA-seq (Supplementary Figure S1B) and real time-quantitative polymerase chain reaction (RT-qPCR) (Figure 1C) analyses. miR-122-5p, described as liver-derived, accounts for 52% of whole hepatic human miRNome [8]. We analyzed miR-122-5p expression in ALCL biopsies from different tissues and confirmed that miR-122-5p was almost or completely absent in all samples except the liver (Supplementary Figure S1C). Moreover, in a panel of ALCL cell lines, miR-122-5p was not expressed, while alpha mouse liver 12 (AML12) cells and S-EVs showed high miR-122-5p levels (Supplementary Figure S1D). These results strongly suggest that miR-122-5p circulating in plasma S-EVs of ALCL patients is not released by the tumor cells but most likely derives from the liver. In line with these observations, we demonstrated the presence of miR-122-5p only in the non-tumoral CD30$^-$ S-EVs fraction (Supplementary Figure S1E). Interestingly, we observed significantly higher transaminase values at diagnosis in ALCL patients with miR-122-5p levels above the median value (Supplementary Figure S1F). Therefore, we hypothesized that the increased circulating levels of miR-122-5p might result from disease-related liver function impairment in patients with advanced ALCL.

To elucidate the role of miR-122-5p in disease dissemination and aggressiveness, we conducted a sequence-

Abbreviations: ALCL, Anaplastic Large Cell Lymphoma; ALDO A, Aldolase A; ALK+, Anaplastic Lymphoma Kinase positive; AML12, Alpha Mouse Liver 12; CD30, Cluster of Differentiation 30; CM, Conditioned Media; CS, Citrate Synthase; ECAR, Extracellular Acidification Rate; EFS, Event Free Survival; GFP, Green Fluorescent Protein; GLUT1, Glucose Transporter 1; HD, Healthy Donors; MEF-1, Mouse Embryonic Fibroblasts-1; miR-122-5p, microRNA-122-5p; miRNA, microRNA; NC, Negative Control; NPM, Nucleophosmin; PCA, Principal Component Analysis; PKM2, Pyruvate Kinase M2; RT-qPCR, Real-Time quantitative-PCR; sRNA-seq, Small RNA-sequencing analysis; S-EVs, Small Extracellular Vesicles.
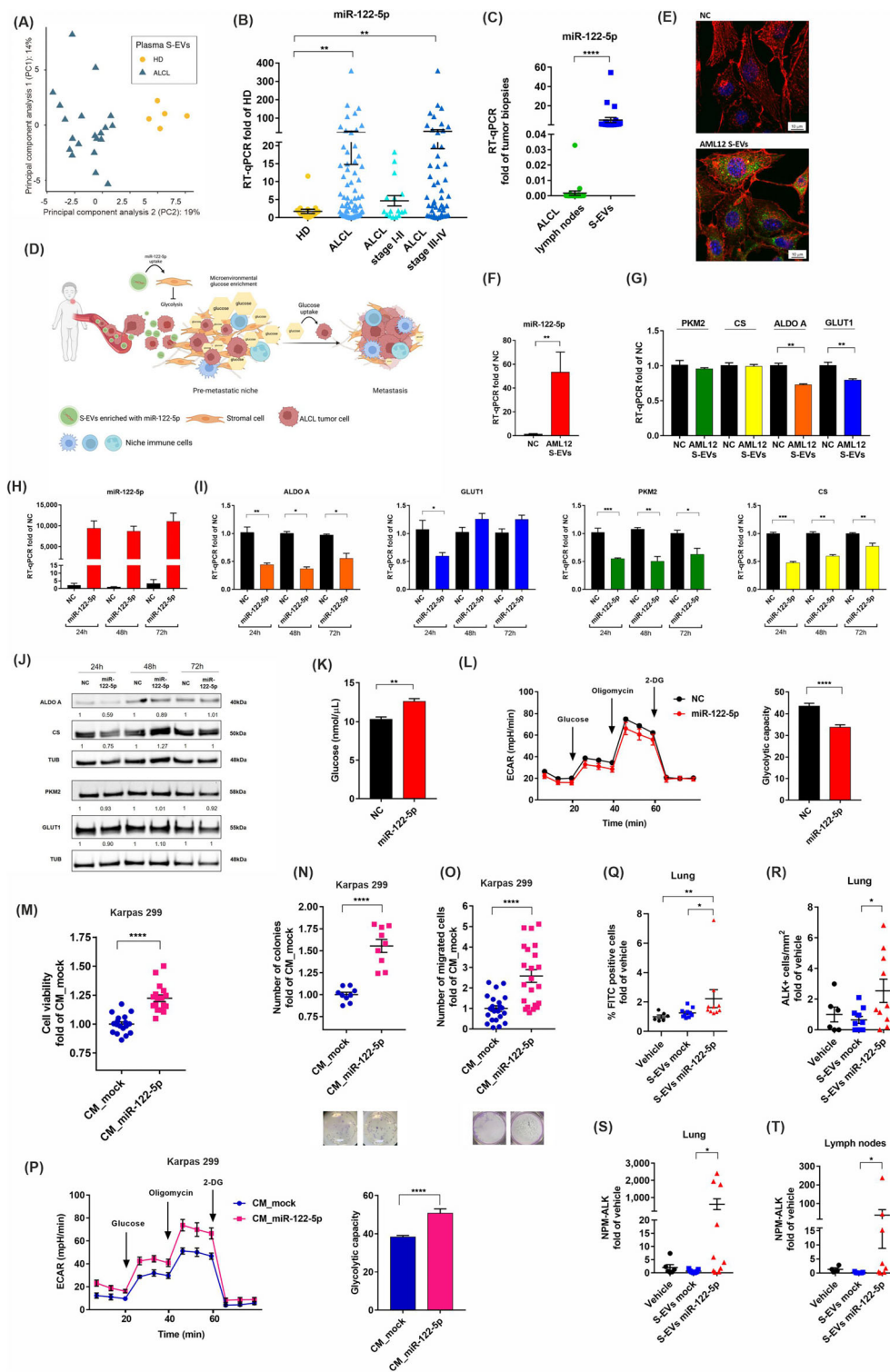
FIGURE 1 Plasma small-extracellular vesicles enriched in miR-122-5p promote pediatric ALCL. (A) Principal Component Analysis (PCA) computed on expression profiles of miRNAs on plasma S-EVs of ALCL and HD from sRNA-seq data, 5 HD and 20 ALCL samples were analyzed (in X-axis Principal Component 1 -PC1- is showed, the variation explained by PC1 is 19%; in Y-axis Principal Component 2 –PC2- is shown, the variation explained by PC2 is 14%). (B) Dot plot showing miR-122-5p expression by RT-qPCR in plasma S-EVs of HD ($n = 19$) and pediatric ALCL ($n = 66$), data have been calculated according to the comparative ΔCt method and compared to HD samples, ALCL patients were displayed all together or according to disease stage (stage I-II $n = 16$; stage III-IV $n = 50$). Of note, the extended cohort of 66 ALCL samples included 49 independent ALCL cases and 17 ALCL patients used in the small RNA-seq analysis. (C) Dot plot showing miR-122-5p expression by RT-qPCR in paired ALCL tumor biopsies ($n = 20$) and plasma S-EVs ($n = 20$), using data calculated according to the comparative ΔCt method and compared to S-EVs samples. (D) Model of pediatric ALCL patients under impaired hepatic functions and high levels of miR-122-5p secretion in plasma S-EVs from the liver. Increased circulating miR-122-5p reduces the glycolytic rate in stromal cells by

based miRNA target prediction with TargetScan (http://www.targetscan.org/). Our results showed that pyruvate metabolism and glycolysis were the most enriched pathways that involved miR-122-5p targets (Supplementary Figure S2). miR-122-5p validated targets are citrate synthase (CS), pyruvate kinase M2 (PKM2) [7] and aldolase A (ALDO A) [9]. We hypothesized that liver-derived S-EVs enriched in miR-122-5p could sustain ALCL dissemination by inhibiting glycolysis in niche cells, thus increasing glucose availability to support cancer cell seeding (Figure 1D). When we treated mouse embryonic fibroblast-1 (MEF-1) as a niche cell model with AML12-derived S-EVs (S-EVs isolation in Supplementary Figure S3), we observed that MEF-1 cells were able to efficiently uptake AML12-derived S-EVs (Figure 1E) and showed increased miR-122-5p intracellular levels compared to control (Figure 1F). Furthermore, S-EVs treatment significantly inhibited the expression of ALDO A (Figure 1G). Moreover, glucose transporter 1 (GLUT1) expression was significantly decreased in cells treated with S-EVs compared to the untreated (NC) group (Figure 1G). We transiently transfected MEF-1 cells not expressing endogenous miR-122-5p with miR-122-5p-mimic (Figure 1H). Significant downregulation of PKM2, CS and ALDO A transcript levels (Figure 1I) was detected in miR-122-5p overexpressing cells at 24, 48 and 72 hours post-transfection. A slight decrease of all miR-122-5p analyzed targets protein was appreciated 24 hours post-transfection (Figure 1J). Moreover, GLUT1 transcript expression was significantly decreased 24 hours post-transfection (Figure 1I), and glucose concentration was increased in MEF-1 cells media overexpressing miR-122-5p (Figure 1K), suggesting that miR-122-5p impacts also on glucose uptake. Moreover, miR-122-5p transfected MEF-1 cells showed impaired glucose consumption, decreased extracellular acidification rate (ECAR) and a significantly lower glycolytic capacity than controls after 24 hours posttransfection (Figure 1L). The results obtained with HEK-293T cells stably overexpressing miR-122-5p (HEK-293T_miR-122-5p) were consistent with those of MEF-1 cells (Supplementary Figure S4). ALCL cells viability was significantly increased upon treatment with conditioned medium (CM) derived from HEK-293T_miR-122-5p (CM_miR-122-5p) compared to the control HEK-293T_mock (CM_mock) (Figure 1M and Supplementary

lowering the expression of its targets (PKM2 and ALDO A). (E) Confocal microscopy images of MEF-1 cells untreated (NC) or treated with AML12-derived S-EVs. Nuclei (blue) were stained with DAPI, cytoskeleton (red) was stained with phalloidin, and S-EVs (green) were stained with Vybrant DiO Cell-Labeling Solution. (F) miR-122-5p levels by RT-qPCR of MEF-1 cells after 6 hours of treatment with AML12 derived S-EVs (250 μg) compared to untreated (NC) cells. (G) PKM2, CS, ALDO A, and GLUT1 transcripts modulation on MEF-1 cells untreated (NC) or treated with AML12 derived S-EVs. Cells were treated three times with 50 μg of S-EVs, and RNAs were collected 24 hours after the last treatment. (H) miR-122-5p expression by RT-qPCR in MEF-1 24, 48 and 72 hours after transient transfection. (I) PKM2, CS, ALDO A and GLUT1 transcripts modulation by miR-122-5p transient transfection after 24, 48 hours and 72 hours in MEF-1 cells. (J) Western blot analysis of PKM2, CS, ALDO A, and GLUT1 in transiently transfected MEF-1 cells 24,48 and 72 hours post-transfection. (K) Glucose quantification in the supernatant of transiently transfected MEF-1 cells 24 hours post-transfection. (L) Left: representative ECAR trace of MEF-1 cells 24 hours after transient transfection; right: glycolytic capacity quantification (maximum ECAR rate – basal ECAR rate) of MEF-1 cells 24 hours after transient transfection. (M) Viability of Karpas 299 cells treated with CM from HEK-293T_mock (CM_mock) or HEK-293T_miR-122-5p (CM_miR-122-5p) for 24 hours, data represent resazurine absorbances compared to the control group. (N) Effect of CM_mock or CM_miR-122-5p on colony formation of Karpas 299, colonies were counted after 10 days, and data are expressed as fold of the control group; below: representative pictures of colonies are reported. (O) Effect of CM_mock or CM_miR-122-5p (48 hours treatment) on the invasion ability of Karpas 299. Invading cells were quantified from bright-field image 10× magnification, and data are expressed as fold of the control group; below are the representative images of invading cells (4×magnification). (P) Left: representative ECAR traces, wherein the X-axis shows the time from the start of the assay (0 min) to the end (70 min); right: quantification of the glycolytic capacity of Karpas 299. (Q) Dot plot representing GFP-positive tumor cells counted by flow cytometry in lungs, data were expressed as fold of vehicle group (vehicle $n = 6$, S-EVs mock $n = 10$, S-EVs miR-122-5p $n = 10$). (R) ALK staining by immunohistochemistry of mice's lung, ALK-positive cells per square unit area were calculated, and data were then expressed as fold of vehicle group. (S) *NPM-ALK* expression in the lung by RT-qPCR, data have been calculated according to the comparative ΔCt method and compared to vehicle group. (T) *NPM-ALK* expression in lymph nodes by RT-qPCR, data have been calculated according to the comparative ΔCt method and compared to vehicle group; experiments were performed three times in triplicate (experiments in panel D and G were performed two times). *P<0.05; **P<0.01; ***P<0.001; ****P<0.0001. Mann Whitney test or unpaired Student's t test have been used for statistical analysis. Data are expressed as mean $\pm$ SEM.

Abbreviations: ALCL: Anaplastic Large Cell Lymphoma; ALDO A: Aldolase A; ALK: Anaplastic Lymphoma Kinase; AML12: alpha mouse liver 12; CM: Conditioned Media; CS: Citrate Synthase; DAPI: 4',6-diamidino-2-phenylindole; 2-DG: 2-Deoxy Glucose; ECAR: Extracellular Acidification Rate; EFS: Event Free Survival; GFP: Green Fluorescent Protein; GLUT1: Glucose Transporter 1; HD: Healthy Donors; HEK-293T: Human Embryonic Kidney 293T; MEF-1: Mouse Embryonic Fibroblasts-1; miR-122-5p: micro-RNA-122-5p; min: Minutes; miRNA: micro-RNA; NC: Negative Control; NPM: Nucleophosmin; PCA: Principal Component Analysis; PKM2: Pyruvate Kinase M2; RNA-seq: RNA-sequencing analysis; RT-qPCR: Real Time-quantitative PCR; S-EVs: Small Extracellular Vesicles; SEM: Standard Error of the Mean; sRNA-seq: small-RNA sequencing; Tub: Tubulin.

Figure S5A). Also, the treatment with CM from HEK-293T_miR-122-5p transfected with miR-122-5p inhibitor reverted the effect of miR-122-5p on ALCL cell glycolysis and viability (Supplementary Figure S6). Interestingly, CM from MEF-1 cells treated with hepatocyte-derived S-EVs increased ALCL cells' viability (Supplementary Figure S7). Similarly, both the invading and clonogenic potential of ALCL cells significantly increased after treatment with CM_miR-122-5p compared to CM_mock (Figure 1N-O and Supplementary Figure S5B-C). To analyze whether the effect of miR-122-5p contributed to the metabolic rewiring of ALCL cells, we analyzed the ECAR of tumor cells treated with CM_miR-122-5p or CM_mock. ALCL cells showed higher levels of ECAR and glycolytic capacity when treated with CM_miR-122-5p compared with CM_mock (Figure 1P and Supplementary Figure S5D). Overall, these results indicate that miR-122-5p impaired niche cells' glucose utilization, favoring ALCL cells' growth and aggressiveness.

To clarify in vivo the role of miR-122-5p in promoting premetastatic niche formation, mice were subjected to multiple treatments with miR-122-5p-enriched S-EVs (S-EVs miR-122-5p) or negative control S-EVs (S-EVs mock) three times a week for three weeks, GFP-labeled Karpas 299 cells were then injected (Supplementary Figure S8) and, after 20 days, the mice were sacrificed, and their lungs, lymph nodes, livers and spleens were collected and analyzed to assess the tumor cell spread. The presence of tumor cells was determined by flow cytometry. We found a significantly increased number of GFP-positive cells in the lungs of mice treated with S-EVs miR-122-5p compared to S-EVs mock (Figure 1Q). ALK staining confirmed the tumor cell spread in the lungs of mice treated with S-EVs miR-122-5p compared with S-EVs mock (Figure 1R and Supplementary Figure S9). Moreover, we found significantly increased tumor cell-specific *NPM-ALK* transcript levels in the lungs and lymph nodes of mice treated with S-EVs miR-122-5p compared to the S-EVs mock (Figure 1S-T).

In conclusion, we described the miRNA profile of plasma S-EVs from pediatric ALCL patients highlighting the role of miR-122-5p in promoting tumor cell dissemination and aggressiveness, despite its non-tumoral origin. This work underlines that ALCL represents a highly heterogeneous ecosystem where malignant and stromal cells collaborate to sustain tumor aggressiveness. Noteworthily, miR-122-5p antagonists, currently in clinical trials [10], could represent an effective therapeutic target for ALCL pediatric patients with high disease dissemination.

DECLARATIONS
AUTHOR CONTRIBUTIONS
Carlotta Caterina Damanti and Lavinia Ferrone designed and performed in vitro experiments, analyzed data and wrote the manuscript. Enrico Gaffo performed bioinformatic analyses. Anna Garbin, Anna Tosato, Giorgia Contarini, and Ilaria Gallingani contributed to in vitro experiments. Roberta Angioni, Barbara Molon, and Giulia Borile performed the in vivo experiments, imaging and analyzed data. Alessandra Biffi, Elisa Carraro, and Marta Pillon provided patients' clinical data Federico Scarmozzino, Angelo Paolo Dei Tos, and Marco Pizzi performed immunohistochemistry analysis. Francesco Ciscato and Andrea Rasola performed and supervised the OCR experiments. Stefania Bortoluzzi supervised bioinformatic analyses. Federica Lovisa and Lara Mussolin were responsible for the conception and design of the study, data analysis, and supervision. All authors contributed to the manuscript writing.

CONFLICT OF INTEREST STATEMENT
The authors declare that they have no conflict of interest.

DATA AVAILABILITY STATEMENT
All data needed to evaluate the conclusions are presented in the paper or the Supplementary Materials. The raw data of the small RNA-seq results are available in the GEO/SRA repository under the accession identifier GSE209838.

ETHICS APPROVAL AND CONSENT TO PARTICIPATE
This study was approved by the ethics committee of each participating institution (CESC n.4256/AO/17). Written informed consent was obtained from parents or legal guardians before patients' enrollment.

The in vivo study was approved by the Local Ethical Committee and received Ministerial Authorization (n°788/2018-PR released on 10/15/2018).

CONSENT FOR PUBLICATION
Not Applicable

Carlotta Caterina Damanti[1,2,#]
Lavinia Ferrone[1,2,4,#]
Enrico Gaffo[3]
Anna Garbin[1,2]
Anna Tosato[1,2]
Giorgia Contarini[1,2]
Ilaria Gallingani[1,2]
Roberta Angioni[2,4]
Barbara Molon[2,4]
Giulia Borile[2]
Elisa Carraro[1]
Marta Pillon[1]
Federico Scarmozzino[5]
Angelo Paolo Dei Tos[5]
Marco Pizzi[5]
Francesco Ciscato[4]
Andrea Rasola[4]
Alessandra Biffi[1,2]
Stefania Bortoluzzi[3]
Federica Lovisa[1,2]
Lara Mussolin[1,2]

[1]*Maternal and Child Health Department Pediatric Hematology, Oncology and Stem Cell Transplant Center, University of Padua, Padua, Italy*
[2]*Pediatric Research Institute "Città della Speranza", Padua, Italy*
[3]*Department of Molecular Medicine, University of Padua, Padua, Italy*
[4]*Department of Biomedical Sciences, University of Padua, Padua, Italy*
[5]*General Pathology and Cytopathology Unit, Department of Medicine-DMED, University of Padua, Padua, Italy*

Correspondence
Lara Mussolin and Federica Lovisa, Maternal and Child Health Department, Pediatric Hematology, Oncology and Stem Cell Transplant Center, University of Padua, Padua, Italy; Pediatric Research Institute "Città della Speranza", Padua, Italy.
Email: lara.mussolin@unipd.it and federica.lovisa@unipd.it

[#]Co-first authors

ORCID
Carlotta Caterina Damanti https://orcid.org/0000-0002-1422-0149

REFERENCES
1. Piccaluga PP, Gazzola A, Mannu C, Agostinelli C, Bacci F, Sabattini E, et al. Pathobiology of anaplastic large cell lymphoma. Adv Hematol. 2010;2010:345053.
2. Le Deley M-C, Reiter A, Williams D, Delsol G, Oschlies I, McCarthy K, et al. Prognostic factors in childhood anaplastic large cell lymphoma: results of a large European intergroup study. Blood. 2008;111(3):1560–6.
3. Woessmann W, Zimmermann M, Lenhard M, Burkhardt B, Rossig C, Kremens B, et al. Relapsed or refractory anaplastic large-cell lymphoma in children and adolescents after Berlin-Frankfurt-Muenster (BFM)-type first-line therapy: a BFM-group study. J Clin Oncol. 2011;29(22):3065–71.
4. Trino S, Lamorte D, Caivano A, De Luca L, Sgambato A, Laurenzana I. Clinical relevance of extracellular vesicles in hematological neoplasms: from liquid biopsy to cell biopsy. Leukemia. 2021;35(3):661-78.
5. Zhang J, Li S, Li L, Li M, Guo C, Yao J, et al. Exosome and exosomal microRNA: trafficking, sorting, and function. Genom Proteom Bioinform. 2015;13(1):17–24.
6. Gaffo E, Bortolomeazzi M, Bisognin A, Di Battista P, Lovisa F, Mussolin L, et al. MiR&moRe2: A Bioinformatics Tool to Characterize microRNAs and microRNA-Offset RNAs from Small RNA-Seq Data. Int J Mol Sci. 2020;21(5):1754
7. Fong MY, Zhou W, Liu L, Alontaga AY, Chandra M, Ashby J, et al. Breast-cancer-secreted miR-122 reprograms glucose metabolism in premetastatic niche to promote metastasis. Nat Cell Biol. 2015;17(2):183–94.
8. Bandiera S, Pfeffer S, Baumert TF, Zeisel MB. miR-122–a key factor and therapeutic target in liver disease. J Hepatol. 2015;62(2):448–57.
9. Li H, Zhang X, Jin Z, Yin T, Duan C, Sun J, et al. MiR-122 Promotes the Development of Colon Cancer by Targeting ALDOA In Vitro. Technol Cancer Res Treat. 2019;18:1533033819871300.
10. Stelma F, van der Ree MH, Sinnige MJ, Brown A, Swadling L, de Vree JML, et al. Immune phenotype and function of natural killer and T cells in chronic hepatitis C patients who received a single dose of anti-MicroRNA-122, RG-101. Hepatology. 2017;66(1):57–68.

SUPPORTING INFORMATION
Additional supporting information can be found online in the Supporting Information section at the end of this article.